Cloudiness and Marine Boundary Layer Dynamics in the ASTEX Lagrangian Experiments. Part I: Synoptic Setting and Vertical Structure

CHRISTOPHER S. BRETHERTON

Atmospheric Science Department, University of Washington, Seattle, Washington

ROBERT PINCUS

Geophysics Program, University of Washington, Seattle, Washington

(Manuscript received 26 June 1994, in final form 3 January 1995)

ABSTRACT

A goal of the Atlantic Stratocumulus Transition Experiment (ASTEX) southeast of the Azores Islands in the east-central Atlantic Ocean during June 1992 was to examine the coupled evolution of cloud, dynamical, and thermodynamical vertical structure in a marine boundary layer (MBL) air mass as it advected from cold to warm water in the trade winds. In two "Lagrangian" observation periods during ASTEX, an unprecedentedly complete view of MBL and cloud evolution was achieved by nearly continuous aircraft coverage of such an air mass for 36–48 hours using three boundary layer aircraft, supplemented by satellite, ship, and balloon observations.

During the first Lagrangian period, an accelerated stratocumulus to trade cumulus transition occurred in a clean marine air mass. In the second Lagrangian period, a 200-hPa-deep decoupled modified continental MBL persisted with almost no change in structure. Cumulus rising into intermittent stratocumulus were observed throughout the period. The two contrasting ASTEX Lagrangians will allow both direct comparison with MBL models and budget studies with essentially all uncertainty from poorly measured advective tendencies removed.

The authors present the synoptic setting and the evolution of cloudiness as seen from satellite for both Lagrangians, and vertical sections of wind, temperature, mixing ratio, liquid water, droplet concentration, and ozone formed from time series of 17 aircraft soundings during each Lagrangian. In Part II, an analyses of sea surface temperature and surface fluxes, cloudiness, drizzle, and entrainment rate during the Lagrangians are presented.

1. Introduction

One of the principal goals of the Atlantic Stratocumulus Transition Experiment (ASTEX) (Albrecht et al. 1995) was to characterize the evolution of cloudiness and vertical structure in a marine boundary layer (MBL) as it moves over a warmer sea surface. It has been known for many years that stratocumulus cloud sheets tend to form where the ocean is cold compared to the lower troposphere, while cumulus cloud fields with a much lower fractional cloud cover predominate where the ocean is warmer (e.g., Klein and Hartmann 1993). However, the interaction of dynamics, radiative processes, air–sea fluxes, and microphysics that go into determining MBL vertical structure, cloud type, and amount are still not well understood. Hence the parameterization of boundary layer cloudiness has turned into a challenging and important parameterization problem in atmospheric and coupled ocean–atmosphere general circulation models.

Two factors combine to make the eastern subtropical oceans in general—and specifically the ASTEX area (28°–40°N, 16°–25°W) of the northeast Atlantic Ocean—an attractive place to examine MBL cloudiness in the field. First, the relatively steady northerly flow in the trade winds minimizes (but by no means removes) the day-to-day variability in the MBL. Second, climatology suggests that we should typically see a substantial decrease in MBL cloud within a given air mass as it moves southward over warmer water.

The "Lagrangian" strategy during ASTEX was designed to follow and intensively measure the physical and chemical processes and the evolution of cloudiness in a single boundary layer air mass for up to two days. In the two Lagrangian intensive observation periods (IOPs) during ASTEX, a column of air within a convecting MBL was tracked for 36–48 hours. Nearly continuous aircraft coverage using three boundary layer aircraft, supplemented by satellite and ship observations, allowed an unprecedentedly complete view of MBL and cloud evolution during this time. ASTEX was the first boundary layer experiment to successfully tackle the logistical complexities of the Lagrangian approach in a remote ocean region for an extended observation period.

Corresponding author address: Christopher S. Bretherton, Atmospheric Science Department, Box 351640, University of Washington, Seattle, WA 98195.

In section 2, we describe some of the advantages and limitations of a Lagrangian strategy. In section 3, we present the synoptic setting, airmass motion, and satellite overview of the two Lagrangian IOPs. In section 4 we present selected time–height sections based on aircraft soundings. In Part II we present analyses of sea surface temperature and surface fluxes, cloudiness, drizzle, and entrainment rate into the MBL during the Lagrangian IOPs.

The two contrasting ASTEX Lagrangian IOPs allow both direct comparison with column models of the MBL and budget studies with essentially all uncertainty from poorly measured advective tendencies removed. The Lagrangian IOPs were a collaboration between ASTEX and the International Global Atmospheric Chemistry Program's MAGE (Marine Aerosol and Gas Exchange) activity (Huebert et al. 1995). MAGE scientists are analyzing a variety of chemical budgets for the Lagrangian IOPs, including ammonia (Zhuang and Huebert 1995) and sulfur (Blomquist et al. 1995), as well as more inert substances that serve as passive tracers. These analyses complement the view of the physical properties of the MBL presented here.

2. The Lagrangian philosophy

Measuring in detail the properties of a moving air mass is much more expensive than measurements at a fixed ground site. What then are the advantages of the Lagrangian strategy? How do we even define an air mass in the MBL in which turbulent mixing causes individual air parcels to rapidly lose their identity? The idea behind the Lagrangian strategy is that the MBL structure is influenced more by vertical mixing than by horizontal mixing and hence that we should focus on a column of MBL air. To average across the mesoscale structure typically seen in the MBL we might envision this column to be a cylinder of $O(50$ km) radius extending from sea level to the trade inversion. The column is strongly mixed in the vertical but its interactions with neighboring columns due to horizontal mixing are assumed to be weak or negligible. One could also imagine the column to have sidewalls that distort following the horizontal flow at their location, so that in a regime of mean horizontal wind, divergence columns would tend to broaden with time. However, we choose instead to consider a column of fixed radius. Where there is mean horizontal wind divergence or convergence, air is assumed to flow out of or into the column sidewalls.

The advantage of following a column rather than using observations at a fixed location is that there is no need to account for the effects of horizontal advection, which are difficult to reliably determine over the ocean. This removes a major uncertainty in thermodynamic and chemical budgets and expedites comparison with MBL models and parameterizations. The one important parameter needed for both budgets and model comparisons that is not directly measured by the Lagrangian strategy is the mean vertical motion as a function of height. Some indirect techniques for deriving mean vertical motion are discussed in Part II.

How is the horizontal velocity of the column determined? In an MBL column in which the mean horizontal wind velocity is entirely uniform with height, the horizontal column velocity is the wind velocity. However, if there is sufficient vertical mixing, the concept of a moving air column also applied to MBLs in which there is significant vertical shear of the horizontal wind between the base and top of the MBL. In this case we consider a column moving at the mass-weighted vertically averaged horizontal velocity. As air parcels circulate in the vertical, any given parcel is equally likely to be found at all heights in the MBL, so averaged over a turnover timescale, all air parcels will move horizontally at the vertically averaged MBL horizontal velocity. Some horizontal exchange of air through column walls due to vertical shear will take place within a turnover time. The magnitude of this horizontal exchange depends on the vertical shear (which is generally less than 5 m s^{-1} between the top of the MBL and the top of the surface layer) and the turnover timescale (which can vary from less than 1 hour in coastal stratocumulus-capped MBL's and cold-air outbreaks to half a day in trade cumulus cloud fields). For instance, if the upper part of the MBL column is on average moving at a velocity 1 m s^{-1} different from the column mean, and air has a residence time of 6 hours in this layer, then a 20-km-wide strip of this air advects into an adjacent column before vertically remixing. Except where horizontal gradients in MBL properties are large, this horizontal exchange has a negligible effect on MBL structure, and the evolution of a moving MBL air column can be regarded as essentially independent of its neighboring air columns.

The mean air column velocity can be determined by following a balloon that is advected by the horizontal airflow, from aircraft-measured winds or from synoptic-scale analyses. Each of these methods has errors. A balloon samples the air motion only at the level it is flying, not the mean motion averaged over all heights in the MBL. Aircraft-measured winds are subject to systematic drifts, and aircraft wind soundings may sample eddies in which the winds differ by 1–2 m s^{-1} from their values horizontally averaged over a 50-km radius cylinder. Synoptic-scale analyses over data-sparse regions of the oceans may have large wind errors. One independent check of the plausibility of an air column trajectory is to use a passive tracer released at the beginning of the trajectory. The tracer should generally follow the trajectory but will be spread by turbulent dispersion. If the calculated trajectory has only small errors, the tracer should be detectable in low concentration along this trajectory.

3. Experimental design, synoptic setting, trajectories, and satellite observations

The two ASTEX Lagrangian IOPs took place 1600 UTC 12 June–1200 UTC 14 June (the first Lagrangian IOP, denoted L1) and 2200 UTC 18 June–1400 UTC 20 June (the second Lagrangian IOP, L2). These dates can be converted to Julian days by adding 152.

a. Experimental design

For the Lagrangian IOPs to be successful, it was important that the air column being tracked follow a trajectory that kept it within aircraft range of Santa Maria for as long as possible. Continuous aircraft coverage of this air column was maintained using three aircraft [The National Center for Atmospheric Research (NCAR) Electra using double crews, the UK Meteorological Research Flight (UKMRF) C130 and the University of Washington C131a], flying a total of six to seven missions during each Lagrangian IOP. The air column was tracked starting from the R/V *Oceanus,* which was stationed well upwind of the island of Santa Maria (37°N, 25°W), where the aircraft were based and the operations coordinated.

The aim was to choose an air column that passed near but not over Santa Maria. This would maximize use of the C131a, whose range was most limited, but at the same time avoid island effects. A second ship, the R/V *Malcolm Baldridge,* was stationed 1000–1500 km downwind of the R/V *Oceanus* and was directed to steam so as to intersect the air column trajectory about 36 hours after it passed the R/V *Oceanus.*

Trajectory and cloudiness forecasts were made based on the ECMWF (European Centre for Medium-Range Weather Forecasts), NMC (National Meteorological Center), and UKMO (United Kingdom Meteorological Office) operational forecast models. These were used to decide when to initiate a Lagrangian IOP and where to position the upstream and downstream ships. The Lagrangian IOPs relied on accurate trajectory forecasts. This was a concern in a remote marine environment with few nearby observations. Most of the ASTEX upper-air soundings were sent to the Global Telecommunication System in real time and assimilated into the ECMWF operational analyses to improve the analyses and forecasts in the ASTEX region (Albrecht et al. 1995; Bretherton et al. 1995).

To follow an MBL air column, several balloons (constant-volume tetroons) were launched from the R/V *Oceanus* within a half-hour interval at the start of each Lagrangian IOP. Each balloon was ballasted to rise approximately 500–750 m above sea level (usually roughly midheight within the MBL) and was equipped with a GPS (Global Positioning System) receiver that determined the balloon location to within ±10 m in the horizontal and ±100 m in the vertical every five minutes. The balloon transmitted a history of its position for the previous 6 hours to any aircraft with a suitable onboard receiver within a range of approximately 100 km. The strategy was to use the balloon centroid as the air column position. By using several balloons, it was originally hoped that the impact of horizontal turbulent dispersion on the balloon trajectories could be quantified. Seven balloons were launched at the start of L1 and five at the start of L2. The balloon design and performance are described further in Businger et al. (1995).

Careful flight planning and coordination between aircraft was required to maintain coverage. On each mission, an aircraft intersected the trajectory and attempted to locate the balloons using its onboard receiver. It then flew a sequence of vertically stacked legs, followed by a sounding, while drifting downstream along the trajectory. The C130 flew 60-km crosswind legs. The Electra and C131a, which were doing filter sampling requiring a large volume of air from a given level, usually flew L patterns including a 60-km crosswind and a 60-km along-wind leg at each level in the stack. Stacks included a near-surface leg below all clouds, at a height of 30–50 m during the daytime and 150 m at night. One or more legs were usually flown slightly beneath the stratocumulus cloud base (but above the base of cumulus clouds rising into the stratocumulus layer if they were present). Another leg was flown just below the MBL capping inversion, in the middle of the stratocumulus cloud layer if one existed. This was followed by a "porpoising" leg, which undulated through the inversion, and an above-inversion leg.

In a vertically sheared MBL, the balloon velocity might differ from the mass-weighted MBL mean horizontal velocity and provide a misleading trajectory, but in the weak shear typical of the ASTEX MBL, this was only a minor source of error. If no balloons could be found, the MBL-averaged aircraft wind sounding was used for trajectory determination.

The upstream ship also released several halocarbon tracers (Blake et al. 1995) that could be detected at extremely low concentration both in aircraft grab samples and also by a second ship, the R/V *Malcolm Baldridge,* that was to intersect the air column trajectory about 1000–1500 km downwind of the release point. During the Lagrangian IOP, the upstream ship steamed downstream following the trajectory to measure sea surface temperature (SST) and take chemical measurements and soundings. To avoid chemical contamination of the MBL by ship exhaust, the ship stayed at least 100 km upwind of the trajectory position. The air column was unavoidably contaminated by aircraft exhaust, but there is no sign that this significantly affected any results presented here.

b. Balloons, trajectories, and aircraft flight locations

The two Lagrangian IOPs provided contrasting examples of evolving cloud-topped marine boundary layers. Experiment L1 (schematically illustrated in Fig. 1)

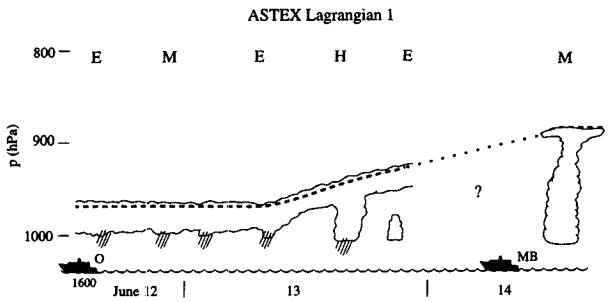

FIG. 1. Schematic of MBL evolution and platform deployment in L1. The air column was followed starting at the R/V *Oceanus* (O at left) until it passed near to the R/V *Malcolm Baldridge* (MB at right) and moved out of aircraft range. Symbols E (Electra), M (C130), and H (C131a) are placed at the midpoint time of each flight. The dashed line traces the approximate inversion pressure, and cloud is stippled. The "?" indicates a 14-hour data gap.

took place in a clean marine air mass with moderate to high wind speeds and low cloud droplet concentrations of 50–75 cm^{-3}. In the first day of L1, the MBL was 70–100 hPa deep, capped by a solid drizzling stratocumulus layer. During the next day the MBL rapidly deepened to a 160-hPa thick layer with cumuli rising into scattered stratocumulus and some deeper cumulus congestus penetrating the trade inversion. During L1, the balloons initially rose above the rather shallow and ill-defined MBL top into higher-velocity winds. They then reentered the MBL and promptly sank into the ocean within about 4 hours of their release, probably due to drizzle loading. After the balloons sank, aircraft-measured wind velocities were used to determine the airmass trajectory, but 28 hours into the experiment poor visibility at Santa Maria forced a 14-hour gap in aircraft coverage. Extrapolation of aircraft winds and the ECMWF forecast were used to estimate the trajectory during the gap, but it remains rather uncertain. Figure 2 shows the "best-guess" trajectory, along with the location of the 17 aircraft soundings used for the time–height sections in section 4, the forecast trajectory (based on averaging 1000-hPa and 850-hPa winds from the ECMWF forecast initialized on 1200 UTC on the day before the experiment), and a trajectory based on 1000-hPa winds from ECMWF operational analyses, which were made every 6 hours. The forecast trajectory was fairly accurate, but after 24 hours, forecast winds appeared to be slightly more northerly than observed. The trajectory from the ECMWF analyses had even more northerly winds. It was also distinctly slower than the best-guess trajectory, especially from the launch to 1200 UTC 13 June, despite the fact that for the first 28 hours the MBL midheight pressure, 975–990 hPa, was quite close to 1000 hPa. It is unclear whether these discrepancies are due to errors in the best-guess trajectory or to errors in the ECMWF analyses.

In L2, wind speeds were lower than in L1. The MBL remained a steady 200 mb thick throughout, with cu-

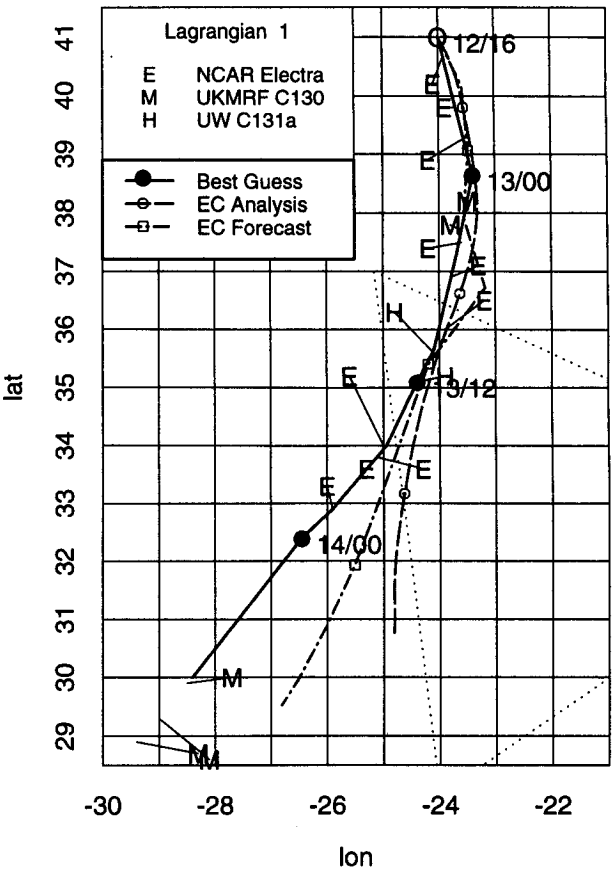

FIG. 2. The best-guess, ECMWF analyzed, and forecast trajectories for L1. Filled circles, hollow circles, and hollow squares indicate the three trajectory positions every 12 hours, with times indicated to the right of the best-guess trajectory. The O indicates the R/V *Oceanus* balloon launch location. The line segments connect the 17 aircraft sounding locations to the contemporaneous trajectory locations.

mulus clouds rising into a thin stratocumulus layer modulated by the diurnal cycle (Fig. 3). Only spotty precipitation was observed despite the vigorous deep cumuli. The air mass had an upstream trajectory from over Europe and contained relatively high aerosol concentrations. Five balloons were released within a 1-

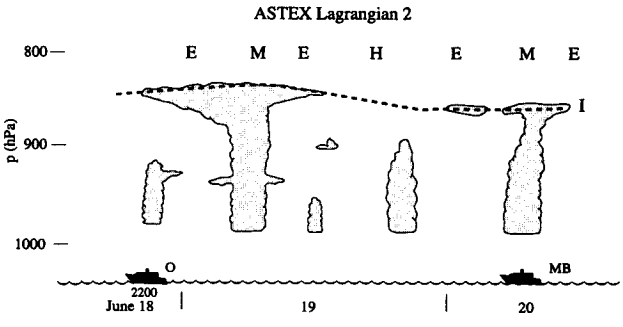

FIG. 3. Schematic of MBL evolution and platform deployment in L2, as in Fig. 1.

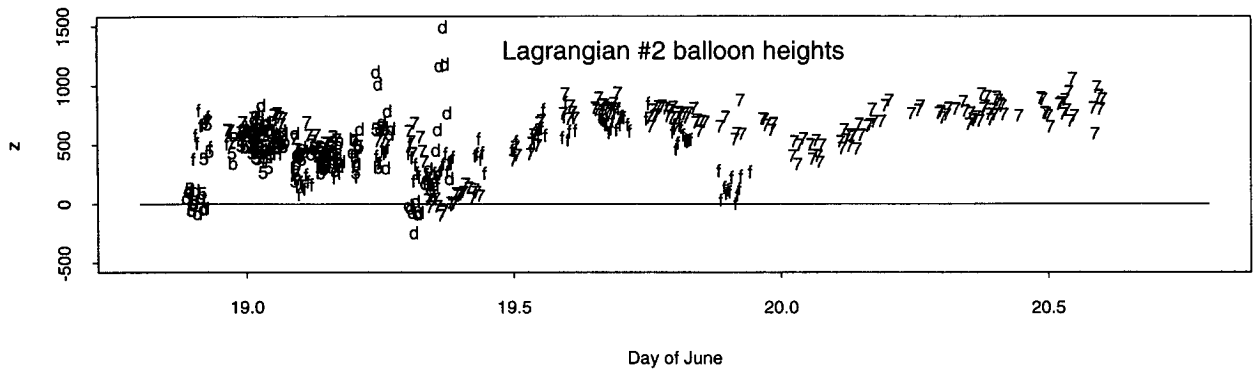

FIG. 4. The GPS-deduced balloon altitudes for the five balloons [5, 7, 11 (b), 13 (d), and 15 (f)] in L2.

hour interval after 2200 UTC 18 June. The ballast weight for three of these balloons was enclosed in a plastic bottle hanging on the end of a 10-m-long string suspended from the balloon. If a balloon neared the water due to a strong downdraft or water loading, the bottle would hit the water and float. The reduced ballast weight would help prevent the balloon from sinking to the ocean surface before it regained buoyancy. While a balloon dragging along the surface for hours would deviate from the desired air column trajectory, this ballasting procedure might save the balloon from a terminal encounter with the sea surface. Figure 4 shows the GPS-reported balloon altitudes in L2. All five balloons had remarkably similar height trajectories considering they were released at several times. Only two of the balloons (one bottle ballasted and one conventionally ballasted) survived an apparent encounter with a precipitating convective line at 0800–0900 UTC on 19 June. Balloon 7 (bottle ballasted) was followed for the entire 40-hour period with continuous aircraft coverage. While the heights in Fig. 4 suggests that balloon 7 may have briefly dragged on the water, there was no evidence in its GPS positions of significant slowing during its one close approach to the ocean surface. Furthermore, its trajectory closely approximated the surviving conventionally ballasted balloon ("f" in Fig. 4) during this encounter. Thus, balloon 7 was used for the best-guess trajectory for L2.

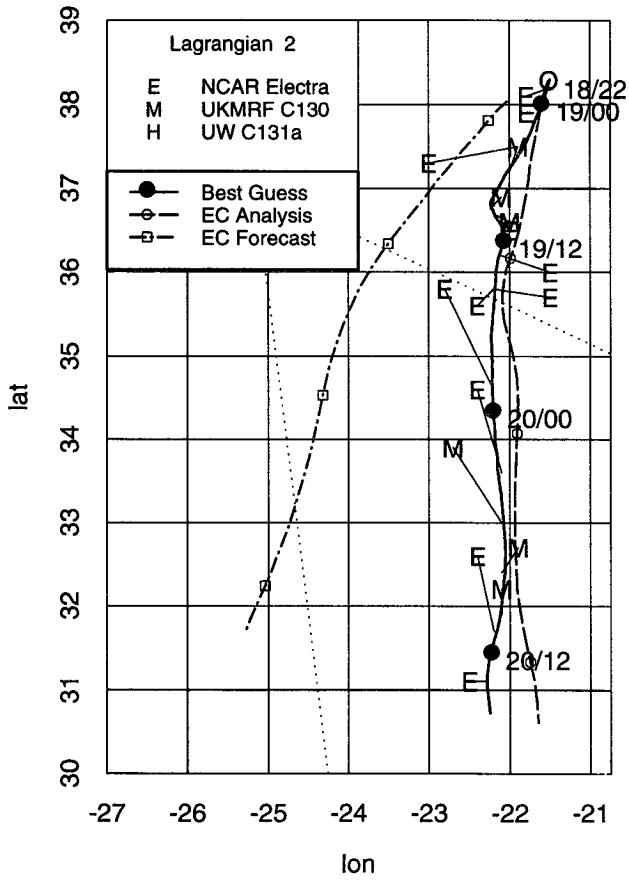

FIG. 5. As in Fig. 2 but for L2.

Figure 5 shows this trajectory, the locations of the 17 aircraft soundings taken during L2, and the ECMWF forecast and analyzed trajectories. The balloon trajectory diverged well to the east of the forecast trajectory, requiring the downstream ship to steam eastward at maximum speed to intersect the trajectory at about 1000 UTC 20 June. Much of the error in the forecast trajectory can be traced to a poorly forecast cyclonic kinking of the trajectories early on 19 June under a weak upper-level disturbance moving northeastward across the trajectory. The L2 trajectory based on ECMWF 1000-hPa analyses was very accurate. This may reflect additional upper-air data that were assimilated into these analyses, including 6-hourly soundings from the R/V *Oceanus*—which in L2 trailed the balloon by only 100 km over the entire trajectory—as well as soundings from the vertices of the ASTEX triangle.

c. *Synoptic setting and satellite coverage of the Lagrangian IOPs*

Figure 6 shows the ECMWF analyzed 1000-hPa geopotential height field and *Meteosat-3* visible imagery at 1200 UTC on 13 June, midway through L1.

At this time, strong flow at 10 m s^{-1} from the NNE, which typified the entire period of L1, was advecting a solid stratocumulus layer over the upper third of the ASTEX triangle. An "O" indicates the position of the air column studied during L1, which was fully cloud covered. Before reaching the R/V *Oceanus* at 41°N, 24°W, this air column had been part of a marine air mass moving eastward across the North Atlantic. After it reached L1, it turned southward and followed the trajectory shown in Fig. 6. Toward the end of L1, a weak upper-level disturbance moved northeastward over the trajectory and may be responsible for the substantial MBL deepening and observations of cumulus congestus observed in the last flight of L1.

In Fig. 7, another satellite perspective on L1 using a sequence of Meteosat IR images is shown. Square "postage stamp" images approximately 256 km on a side for four times during L1 are shown. Each postage stamp is centered on the trajectory location at the time of the image. During the first 20 hours of L1 there is solid low cloud cover. Later, breaks develop, along with patchy colder cloud tops that suggest penetrating cumulus convection.

Figures 8 and 9 show the satellite view of L2. At 1200 UTC 19 June (15 hours into L2), much of the ASTEX study region (including the trajectory) is overlain by cirrus associated with an upper-level cyclonic circulation, with patchy stratocumulus below, as Fig. 8 shows. The two middle IR postage stamps for L2 (Fig. 9) are affected by this cirrus coverage. During L2, the IR brightness temperatures reported by the Meteosat sensor (as calibrated by the University of Wisconsin) for boundary layer clouds are lower than the in situ measurements of cloud top temperature by 2–5 K.

Figure 10 shows satellite-derived cloud properties retrieved during the daylight hours of L1 and L2. A bidirectional reflectance algorithm is used to convert the visible channel radiance in each pixel (of about 5 km on a side) into a reflectance. The reflectance is defined to be the albedo if both the satellite and sun are at the zenith. We identify a pixel as being cloudy if the reflectance exceeds 0.12, and clear otherwise. For a sea surface albedo of 0.07 overlain by a homogeneous layer cloud, this threshold corresponds to a cloud optical depth of 2. The cloud fraction is defined to be the fraction of cloudy pixels in a postage stamp centered on the current air column position. Horizontal intrapixel variations in cloud and sea surface albedo and sensor noise make the interpretation of reflectances below the threshold of 0.12 in terms of cloud fraction and optical properties rather uncertain. We examine the sensitivity of our results to the choice of threshold by determining cloud fraction with threshold values of 0.08 and 0.15, as indicated by the vertical lines. During L1 cloud fraction remains near 1 regardless of the threshold chosen, but during L2 the cloud fraction is quite sensitive to threshold value, indicating a large uncertainty in retrieved cloud fraction. During the first day of L2 the low clouds are somewhat obscured by the optically thick cirrus aloft; we determine the properties of the boundary layer clouds alone by excluding those pixels with infrared brightness temperatures colder than 275 K.

We retrieve the optical depth (at 0.6 μm) of cloudy pixels using a lookup table method (Pincus et al. 1994). The optical depths shown during L1 (day 13) correspond to liquid water paths of 40 g m^{-2} such as would be seen in a 200-m-thick stratocumulus cloud with adiabatic liquid water content thick. The optical depths retrieved during both days of L2 are consistent with solid cloud about 100 m thick but are more likely due to broken clouds with cell dimensions smaller than a pixel.

4. Aircraft-derived time–height sections

The soundings from all three aircraft taken from within 150 km of the moving air column position were merged to form time–height cross sections of MBL evolution. Potential temperature θ and vapor mixing ratio q_v, droplet concentration, and liquid water content were compiled for all soundings. Droplet concentrations were tabulated from the Particle Measurement Systems (PMS) Forward-Scattering Spectrometer Probe (FSSP) onboard each aircraft, which counted particles in 15 bins spanning radii of 1.3–33.1 μm (Electra), 1–23.5 μm (C130), and 2–30 μm (C131a). The liquid water content compiled for the Electra and C131a were based on the FSSP measurements, while the C130 liquid water contents are derived from their total water probe. The O_3 measurements were available from the Electra and C131 as fast ozone sensors. Winds were obtained only for the Electra and C130 soundings.

Some variables, such as liquid water content, are quite horizontally inhomogeneous. The degree of horizontal inhomogeneity can be gauged from the differences between pairs of soundings at closely spaced times. For such variables, a series of time–height sections based on individual soundings cannot be expected to represent the time evolution of the horizontal averages of these variables across a 50-km wide air column.

a. Lagrangian IOP 1

Figure 11 shows time–height sections of winds during L1 averaged over 40-hPa layers from the Electra and C130 soundings. There is little indication of significant wind shear in the MBL. On a few early soundings in L1 there is up to 5 m s^{-1} easterly shear through the capping inversion, but in general the shear is weak both through and above the inversion. Figures 12 and 13 show potential temperature θ and vapor mixing ratio q_v during L1, based on all aircraft soundings vertically averaged over 10-hPa intervals with no time smoothing. Soundings taken within a few hours and within 100–200 km of each other were quite reproducible except for mesoscale variations of 0.2 K, 0.5 g kg^{-1}, and 10 hPa in inversion height. We have not interpolated across the nearly 14-hour data gap during the night of 13–14 June.

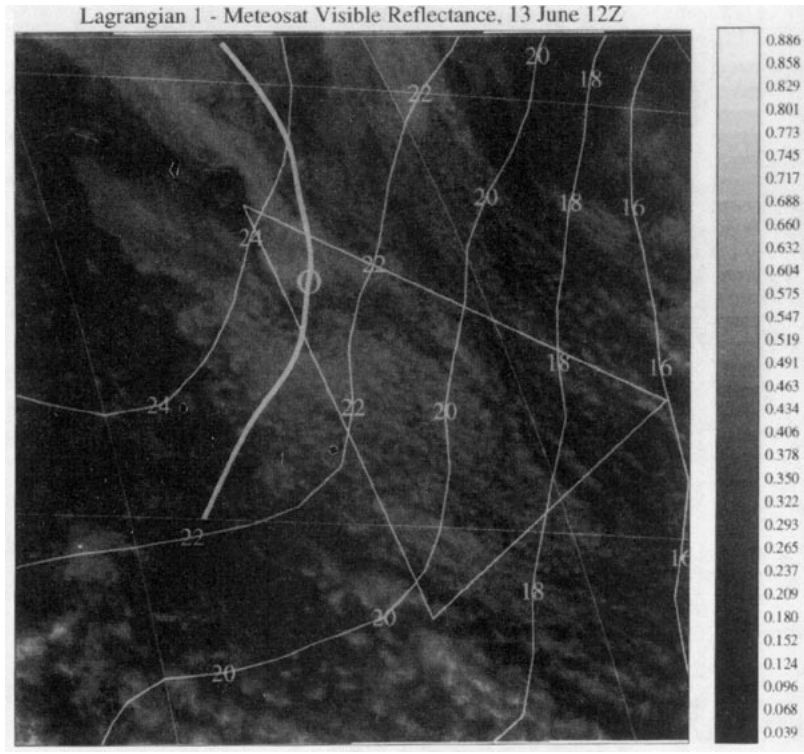

FIG. 6. Meteosat visible satellite imagery at 1200 UTC on 13 June, midway through L1. Contours indicate the ECMWF-analyzed 1000-mb geopotential height field (m); the thick gray line shows the best-guess trajectory. An O denotes the approximate air column position at the time of the image.

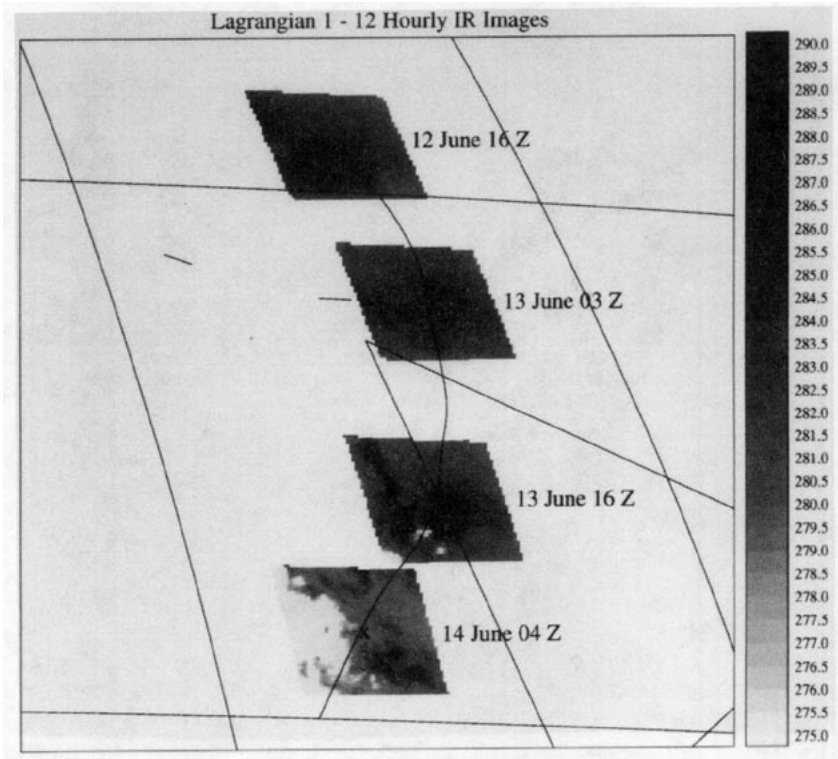

FIG. 7. The 256 km × 256 km Meteosat IR brightness temperature over four postage stamps centered on the contemporaneous L1 trajectory location (×).

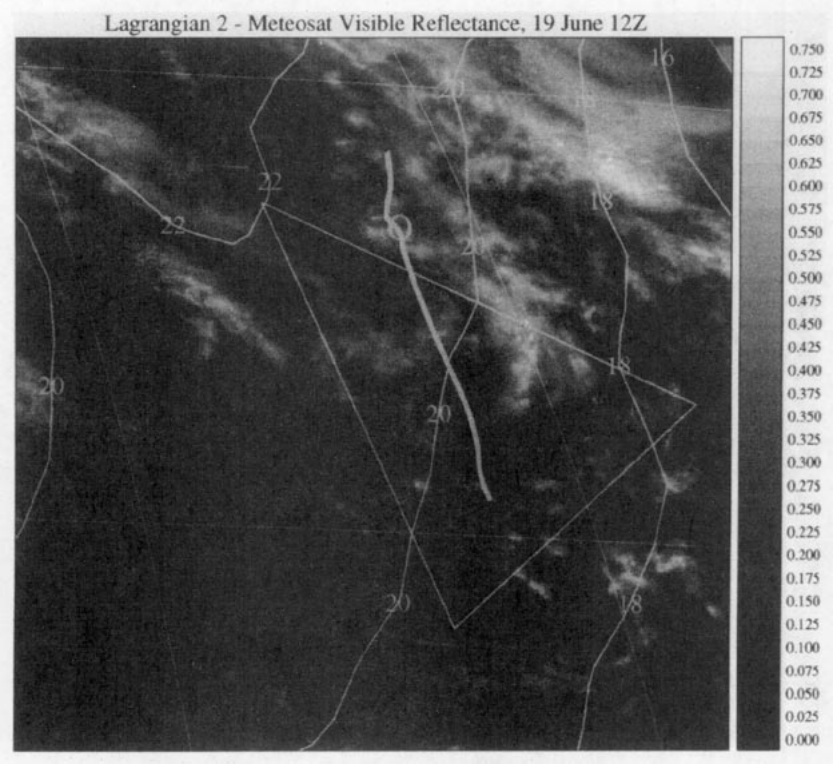

FIG. 8. As in Fig. 6 for L2 at 1200 UTC on 19 June.

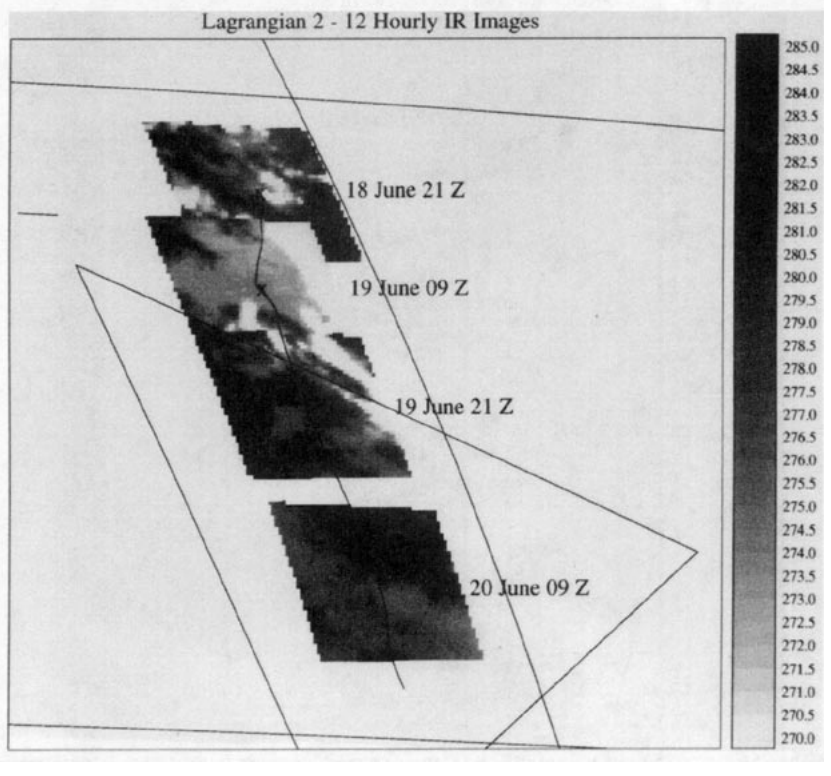

FIG. 9. As in Fig. 7 for L2. Note that the temperature scale is 5 K colder than in Fig. 7.

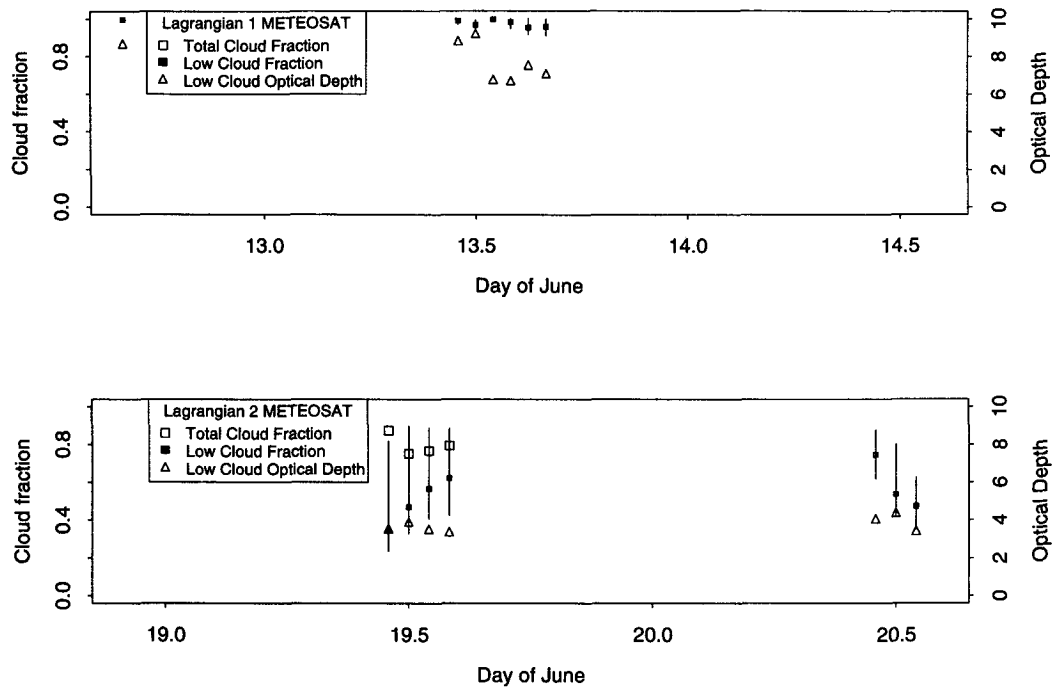

FIG. 10. Satellite-derived cloud fraction and cloud optical depth for L1 and L2, using a visible reflectance threshold of 0.12. Vertical lines denote the range of boundary-layer cloud fractions determined by using reflectance thresholds of 0.08 and 0.15; boundary-layer clouds in L2 are those with brightness temperatures exceeding 275 K. Total cloud fractions are plotted only at times for which there are pixels with brightness temperatures less than 275 K in the postage stamp.

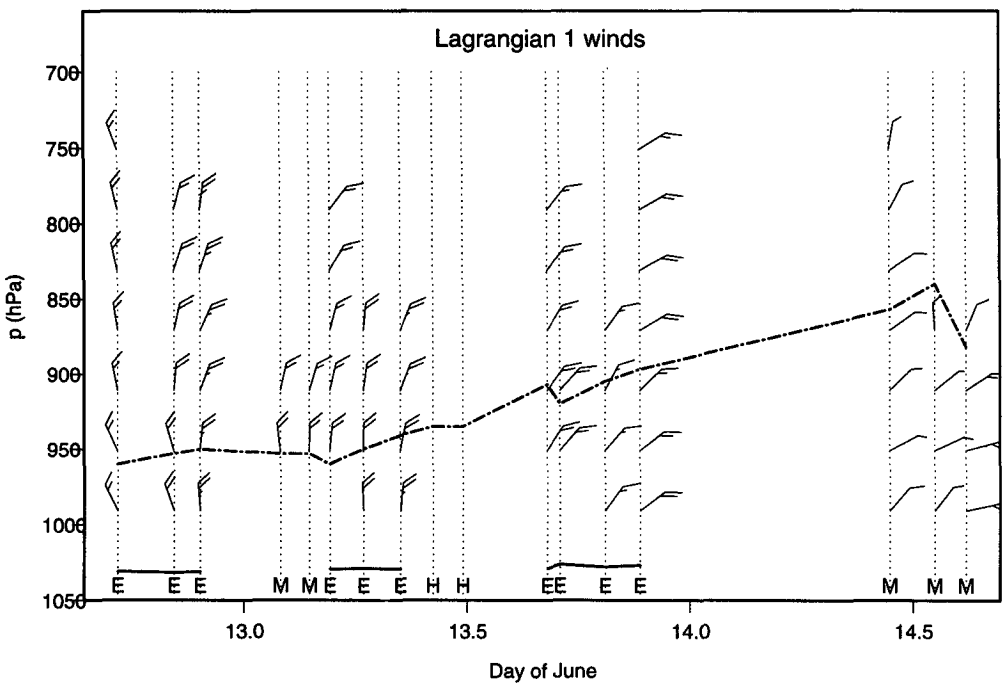

FIG. 11. Time–height sections of winds during L1 averaged over 40-hPa layers from Electra and C130 soundings. Each full wind barb corresponds to 5 m s^{-1}. Each sounding is indicated by a vertical dashed line with an aircraft identifier (see Fig. 2) at its base. The surface pressure (heavy solid line) was computed at the bottom of each Electra sounding from the pressure and radar altitude. The inversion base (heavy chain–dashed line) is taken to be the height of the local minimum in temperature in each sounding.

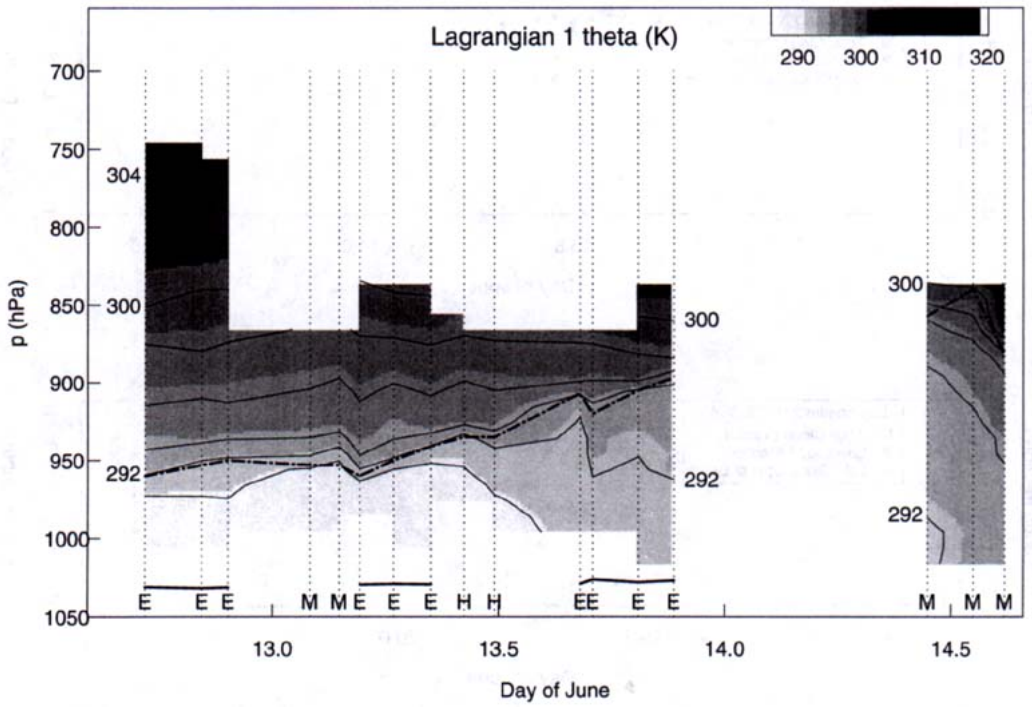

FIG. 12. The θ (contours every 2 K) during L1 averaged over 10-hPa layers, based on all aircraft soundings. Other symbols are as in Fig. 11.

A 2–4 K inversion was evident in all soundings. There was initially no jump in mixing ratio at the inversion; during 13 June the jump became well defined as the MBL rapidly deepened. The ECMWF operational analysis (not shown) retained a shallow MBL along the entire trajectory, perhaps as a result of the

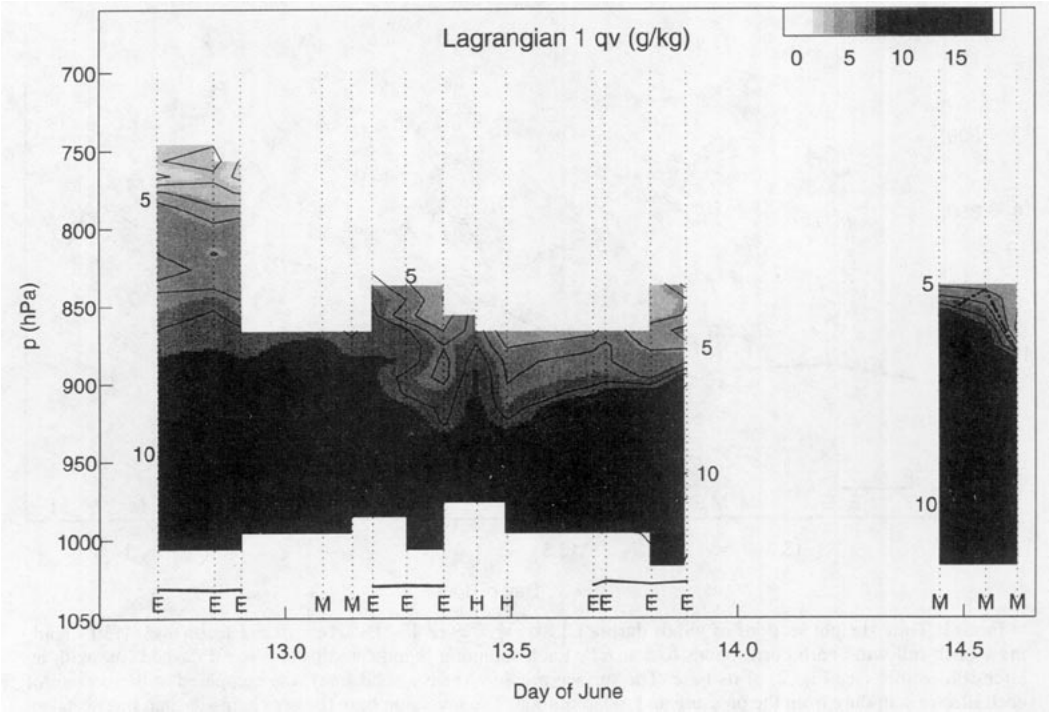

FIG. 13. The q_v (contours every 1 g kg^{-1}) during L1 as in Fig. 12.

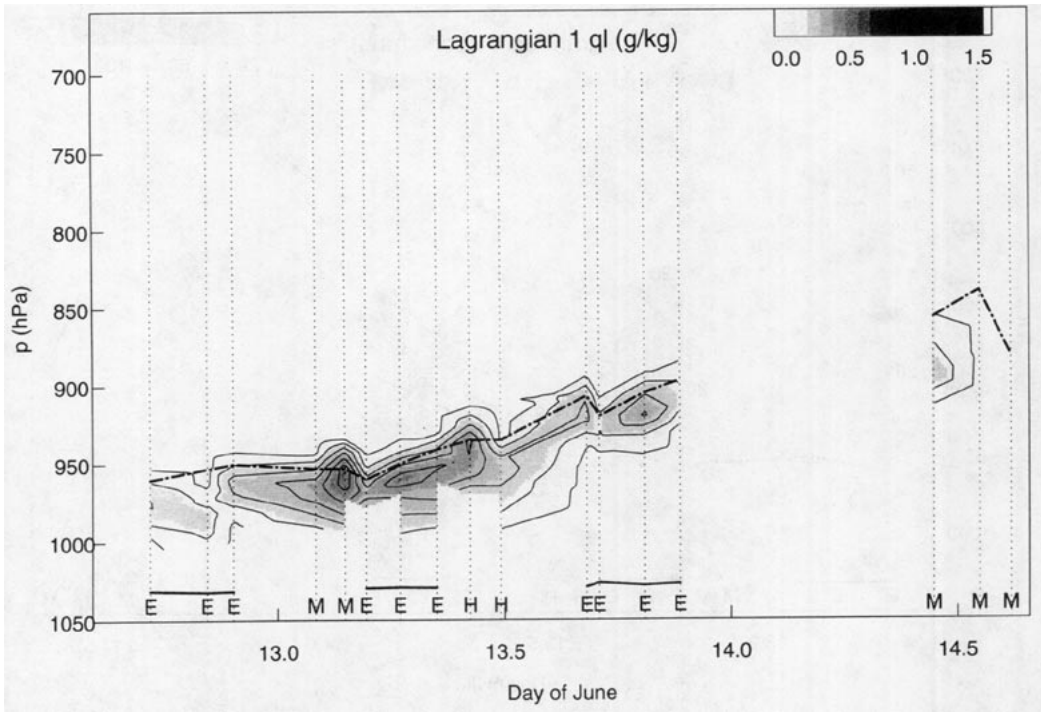

FIG. 14. Cloud liquid water (contours at 0.02 and every 0.1 g kg^{-1}) for L1 as in Fig. 12.

sparsity of upper-air soundings in this region. (Soundings from the downstream ship were transmitted to ECMWF too late to meet data cutoff times for the ECMWF analysis.) As the boundary layer deepened, a transition layer at 970–990 hPa formed. The bases of cumuli that rose into the overlying stratocumulus layer were located in the lower part of this transition layer.

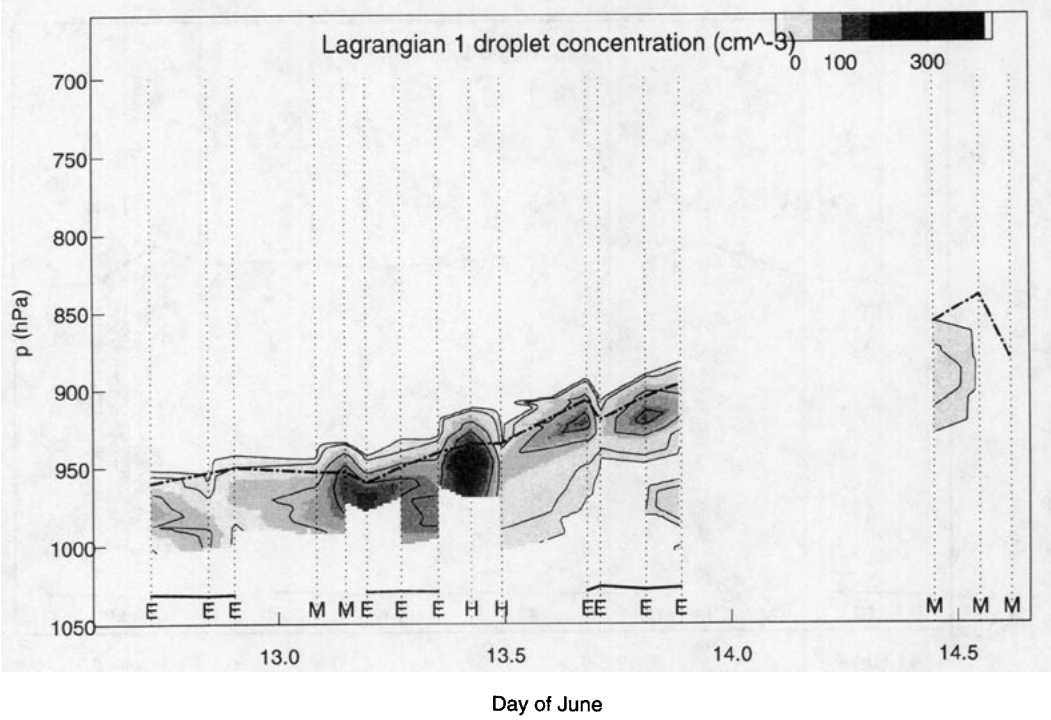

FIG. 15. Droplet concentration (contours at 2, 10, 50, 100, 200, 300, 400 cm^{-3}) for L1 as in Fig. 12.

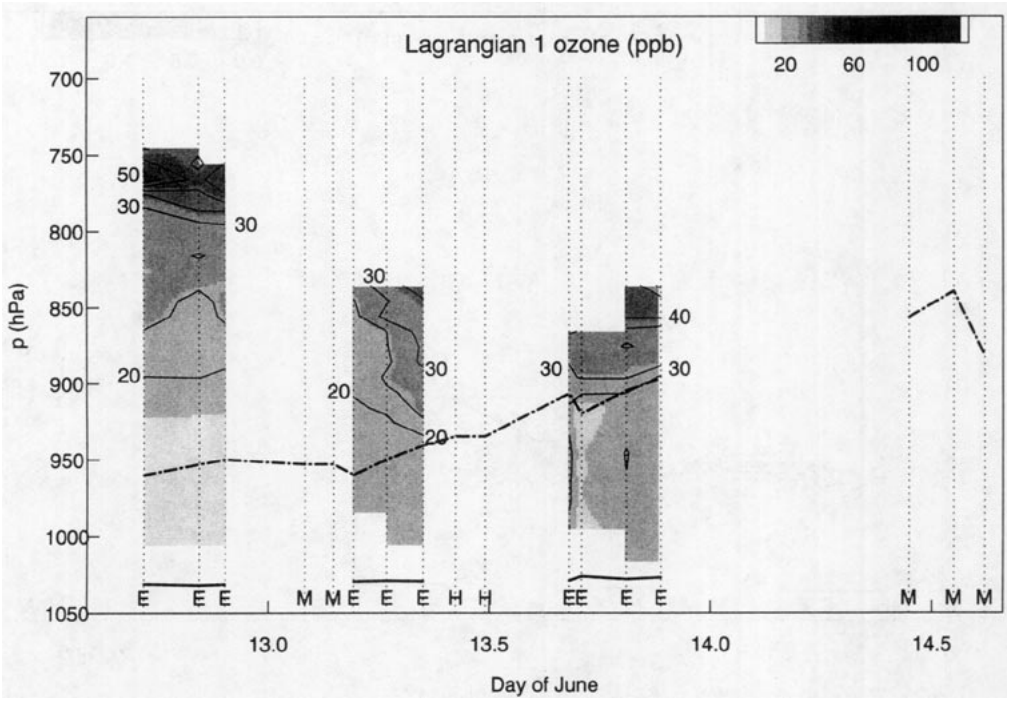

FIG. 16. The O_3 (contours every 5 ppb) for L1 from Electra soundings as in Fig. 12.

Sections of cloud liquid water (Fig. 14) and droplet concentration (Fig. 15) show that in the first 24 hours of the first Lagrangian IOP, the MBL was capped by stratocumulus with a low cloud base and droplet concentrations between 50 and 150 cm^{-3} (consistent with the mid-Atlantic back-trajectory of this air mass). The first C131a sounding showed higher droplet concentrations, up to 250 cm^{-3}. The C131a may have flown

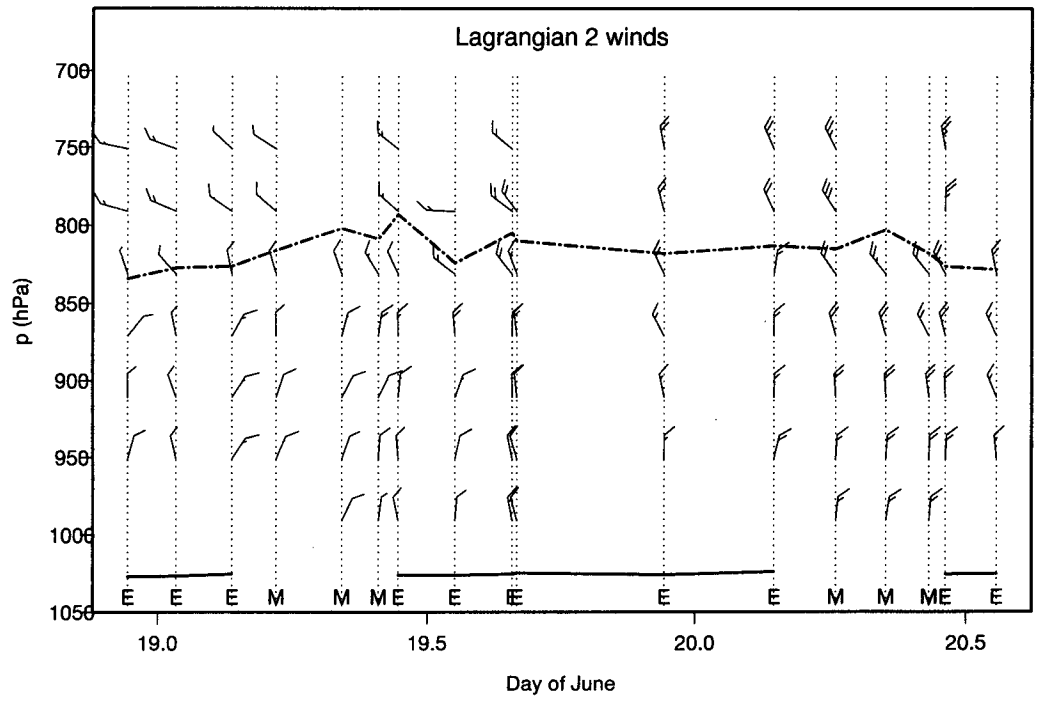

FIG. 17. Wind section for L2 as in Fig. 11.

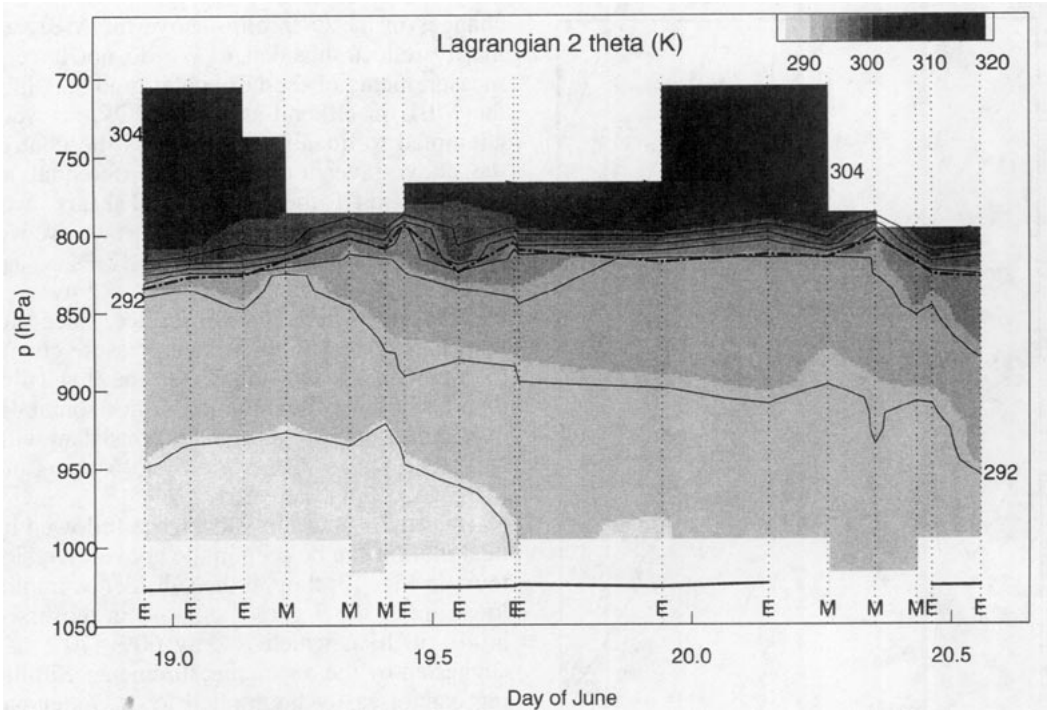

FIG. 18. The θ section for L2 as in Fig. 12.

through dilute aircraft exhaust, but large mesoscale variability in droplet concentration in solid cloud was also apparent on horizontal flight legs, perhaps due to local drizzle scavenging. The stratocumulus became more patchy in the deeper MBL sampled by the C130 flights on the morning of 14 June. Note that cloud with a 10-hPa average liquid water content of 0.02 g kg^{-1} liquid water content or less is not plotted in Fig. 14.

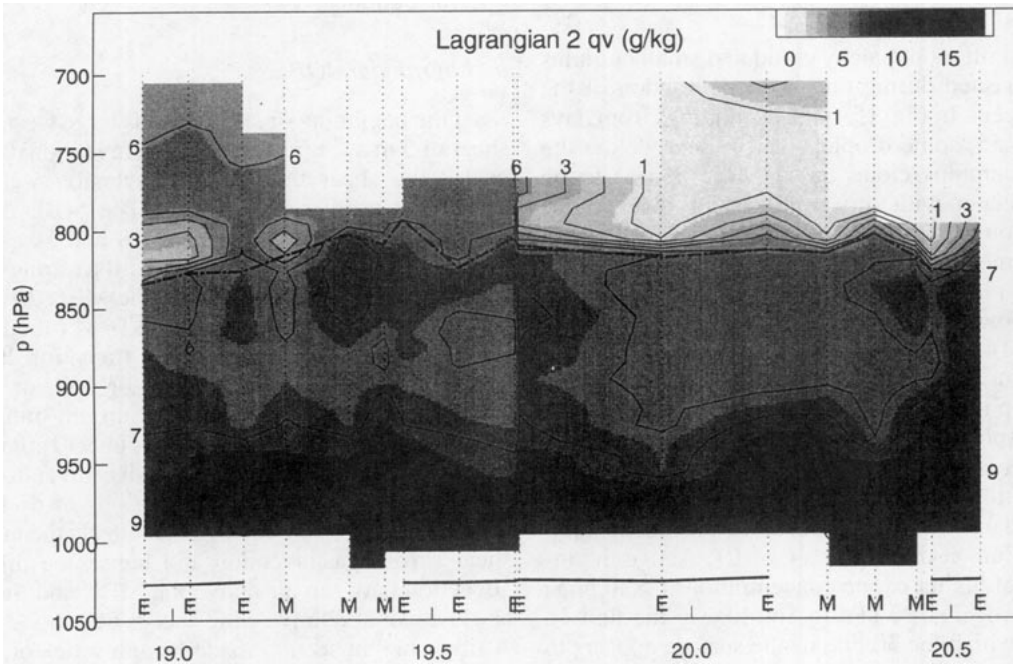

FIG. 19. The q_v section for L2 as in Fig. 13.

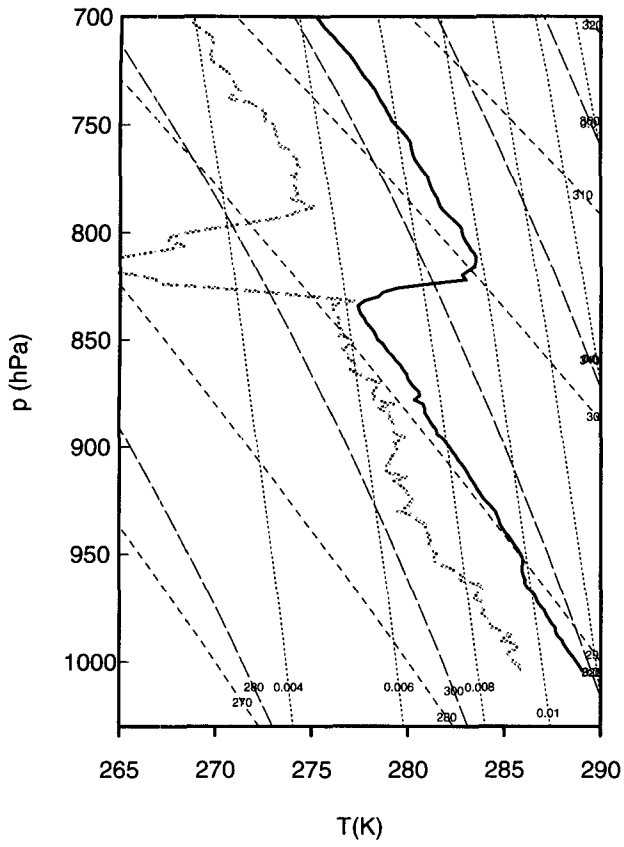

FIG. 20. The T (heavy dark curve) and T_d (light curve) from sounding 1 of L2 (Electra, 2240 UTC 18 June). The background lines are isopleths of mixing ratio (short dashed), dry adiabats (medium dashed), and moist adiabats (long dashed).

This tends to filter out patchy cloud and small cumulus clouds intersected during only a small fraction of the sounding ascent. In Fig. 15, on the soundings from days 13.9 and 14.55, some droplets can be seen below the main stratocumulus cloud base. These appear to be mostly associated with very small "scud" or cumulus clouds. Although the different types of cloud liquid water measurement used aboard the two aircraft might have led to platform-dependent biases, these did not stand out above the natural variability between soundings in Fig. 14.

Ozone is an approximately conserved trace gas, with only weak photochemical sources and sinks in the lower troposphere and a sink at the ocean surface. A section of O_3 (Fig. 16) from the Electra soundings indicates very low O_3 concentration (<25 ppb) both in the MBL and up to 850 hPa, with almost no ozone jump at the inversion, at the beginning of L1. Above the inversion, air of higher ozone concentrations (>30 ppb) moved down from 790 hPa to 860 hPa in the first 16 hours, after which the 30 ppb ozone surface appears to have remained at a fairly steady pressure.

If all the air in the free troposphere was moving at the mean MBL horizontal velocity, the temporal changes in the O_3 profile above the MBL would primarily reflect subsidence. We do not have extensive measurements of the horizontal gradients in O_3 above the MBL in either Lagrangian IOP, so we have not attempted to quantitatively assess the contribution to the above-inversion O_3 from differential advection. However, in L1, the vertical wind shear is weak. From the subsidence of the 30 ppb O_3 surface, we would infer a vertical pressure velocity $\omega = 0.12$ Pa s^{-1} (and mean horizontal divergence of 6×10^{-6} s^{-1} over a 200-hPa-thick layer down to the sea surface, since the sea surface ω estimated from surface pressure changes along the trajectory is very small) for the first 16 hours and then no mean vertical motion or horizontal divergence over the next 12 hours. This is consistent with the low MBL heights seen over the first 16 hours of L1 with MBL deepening thereafter.

The same pattern of subsidence followed by no vertical motion can be seen in the above-inversion q_v contours in Fig. 13, though the subsidence implied by the lowering of the 7 g kg^{-1} contour in the first 16 hours is 40–50 hPa, which is only 60%–70% as large as suggested by the ozone measurements. Similar reasoning cannot easily be applied to the latter part of L1, because of the data gap.

We also obtained O_3 measurements from the first C131a sounding. The measured concentrations (not shown) were approximately 30% lower at all height levels than for the Electra sounding from 90 minutes earlier. The two soundings were on opposite sides of the nominal trajectory, so this may reflect horizontal gradients in O_3 or it may reflect measurement biases. The O_3 sensor was not operational for the second C131a sounding.

b. *Lagrangian IOP 2*

At the beginning of L2 there was large westerly wind shear of 5 m s^{-1} through the trade inversion; by the end of L2 the shear through the inversion was equally strong but northerly (Fig. 17). The MBL depth and thermodynamic structure (Figs. 18 and 19) remained remarkably constant with time, with a strong (6–8 K) inversion with slow warming in the MBL driven by an approximately 3-K increase in SST over the trajectory (see Part II). A clearly defined transition layer was seen, separating mixing ratios of 9 g kg^{-1} or more below 990 hPa from 6 to 7 g kg^{-1} mixing ratios in the cumulus cloud layer between about 940 hPa and the MBL top at 800–820 hPa. The above-inversion mixing ratio varied substantially over periods of 6–12 hours, ranging from 1 to 6 g kg^{-1}. This reflects the large wind shear across the inversion and hence the differential advection between air above the MBL and the boundary layer air at relative wind speeds of 5 m s^{-1} or more. A time–height section made from a series of 3-hourly soundings taken from the R/V *Oceanus* (not shown), which was closely following the balloon, was very similar to Figs. 18 and 19 and extended the aircraft sound-

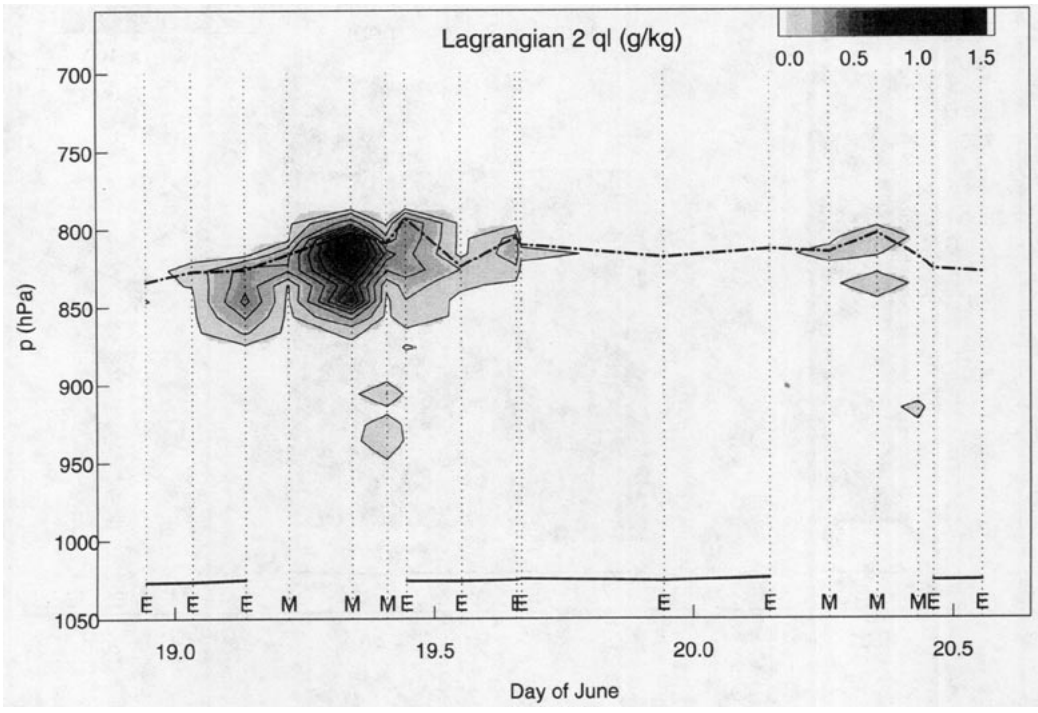

FIG. 21. Cloud liquid water for L2 as in Fig. 14.

ing data into the upper atmosphere; the assimilation of these soundings resulted in a fairly realistic depiction of the MBL and its evolution along the trajectory even in the ECMWF analyses (not shown). It is striking how little the overall MBL thermodynamic structure responded to the large changes in the overlying air, though the cloudiness decreased dramatically as the overlying air dried out between day 19.5 and day 20.

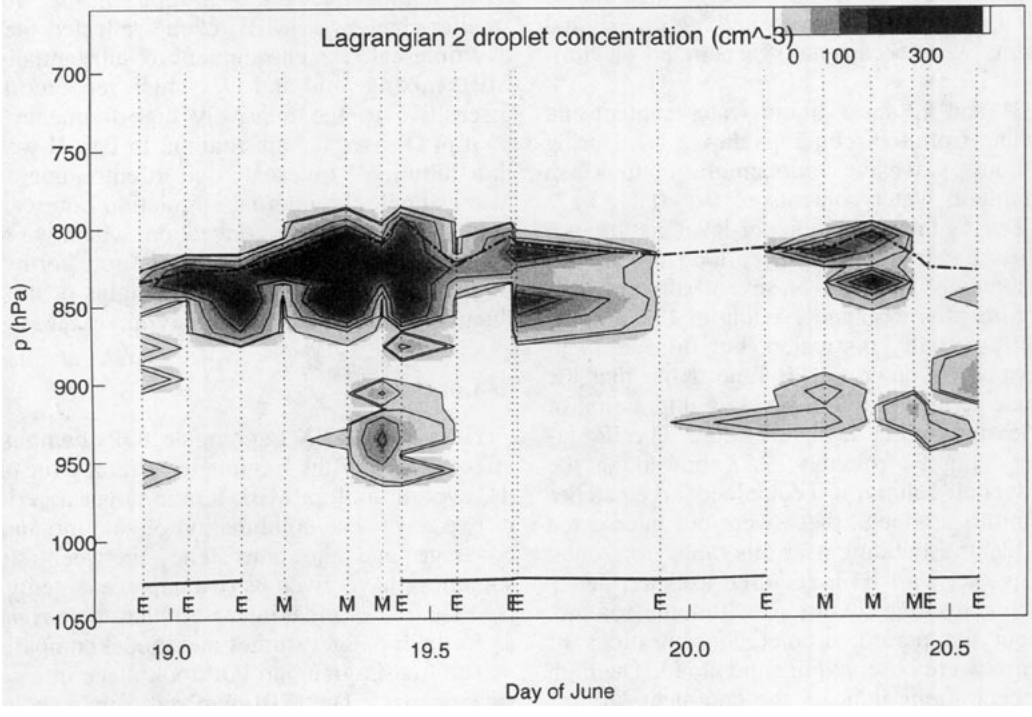

FIG. 22. Droplet concentration for L2 as in Fig. 15.

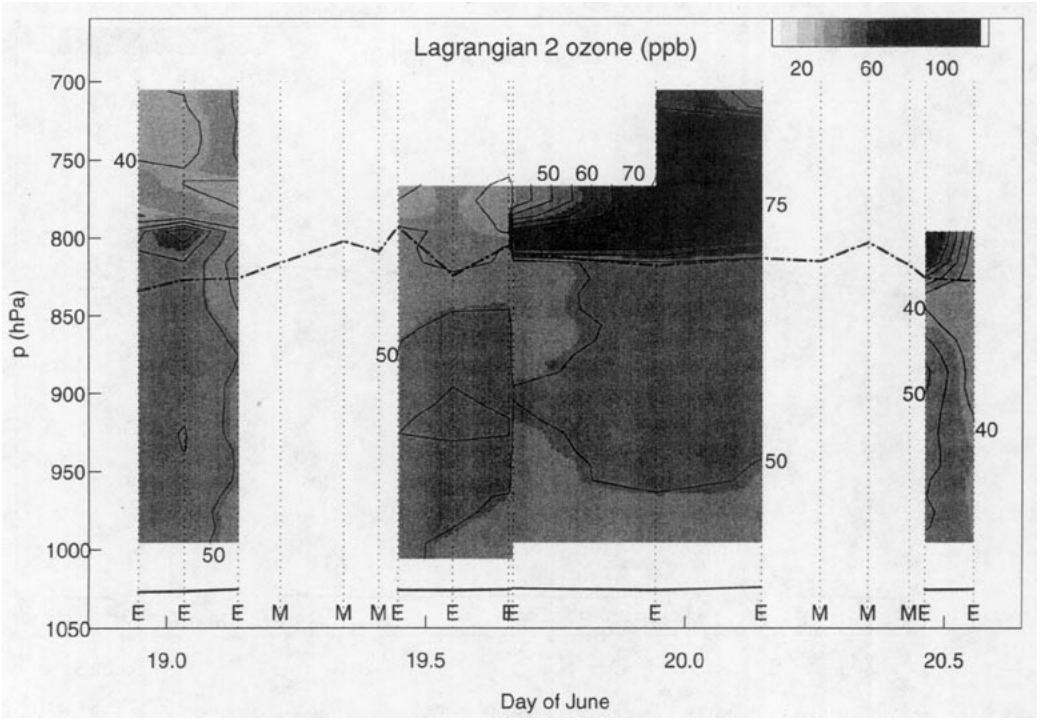

FIG. 23. Ozone for L2 as in Fig. 16.

Figure 20 shows the first aircraft sounding, which is representative of all of L2. The sounding shows a weak temperature increase at 960 hPa in the transition layer and a temperature stratification in the cumulus layer that is closer to dry adiabatic than moist adiabatic, and hence quite conditionally unstable. Indeed, cumulus clouds with up to 5 m s^{-1} updrafts and 5 g kg^{-1} liquid water contents were occasionally penetrated on horizontal legs of L2.

Figures 21 and 22 show liquid water content and droplet number from the soundings during L2. During the first 18 hours, extensive stratocumulus up to 400 m thick, with liquid water contents of 0.1–0.8 g kg^{-1} were seen. During this time an upper-level disturbance moved across the trajectory, the balloon trajectories kinked cyclonically, and five of seven balloons were lost. During the afternoon and evening of 19 June, the stratocumulus partially dissipated, but thin stratocumulus reformed by dawn on 20 June. Note that the sounding time series gives a misleading impression of complete clearing during days 19.7–20.2. The IR satellite imagery (Fig. 9) from day 19.88 showed that the boundary-layer air column still contained large patches of stratocumulus, although these were not intersected by the one Electra sounding near this time. Horizontal leg averaging (see Part II) is required to better determine horizontal average conditions within the column.

Throughout the period, droplet concentrations of 200–300 cm^{-3} were observed in solid cloud. The high droplet concentrations indicate the continental European influence on this air mass. The 1000-hPa back trajectories for the air column (not shown) can be traced back to England 2–3 days before the start of L2.

The O_3 section (Fig. 23) shows large variations (from 40 to 75 ppb) in free-tropospheric ozone concentrations inversely correlated with q_v, and a much more homogeneous 45–55 ppb in the MBL. The smaller changes in MBL ozone reflected the several-day timescale for entrainment to substantially change MBL mixing ratio and O_3, which rendered the MBL insensitive to the relatively high-frequency changes seen in O_3 over the air column. In Part II we quantify the "dilution" timescale due to entrainment, and we also estimate the internal circulation timescale for the MBL due to cumulus convection, which we find to be on the order of half a day. It is noteworthy, though probably coincidental, that the heights of the balloons fluctuated on this same half-day timescale.

5. Conclusions

The two ASTEX Lagrangian IOPs demonstrate the effectiveness of the Lagrangian strategy for observing the evolution of an MBL airmass over a period of up to two days. The combination of satellite and aircraft coverage and the consistency between successive soundings have given us two unprecedentedly detailed case studies, of great interest in their own right as well as for both budget studies and model comparisons.

The first Lagrangian IOP took place in a clean marine air mass. The MBL evolved from a shallow drizzling stratocumulus layer into a trade cumulus layer

with some overlying stratocumulus and some deeper convection in 36 hours. Since winds above the MBL were similar to those in the MBL, we could infer mean vertical motion from changes in the above-MBL profiles of O_3 and water vapor following the MBL air mass. These suggest that mean vertical motion gradually changed from downward to upward during hours 12–36, hastening the MBL deepening and cloud transition. There is some uncertainty in the trajectory and the last 24 hours of MBL evolution, due to a 14-hour data gap and the sinking of the balloons that were to trace the MBL air column motion.

In the second Lagrangian IOP, a 200-hPa-deep MBL with cumulus rising into intermittent stratocumulus and a strong capping inversion of 6–8 K was tracked for 36 hours with almost no change in structure. All vertical profiles show a decoupled structure reminiscent of trade cumulus boundary layers that was typical of the MBL during ASTEX. The air mass had advected from northern Europe 3–4 days earlier. The modified continental nature of this air mass is reflected in droplet concentrations of 150–250 cm^{-3} and may also have contributed to much higher O_3 concentrations both in and above the MBL than were observed in L1. Significant vertical shear at the inversion appears to have driven large variations in q_v and O_3 concentrations above the MBL over periods of just a few hours due to differential horizontal advection, though as in L1 vertical shear within the MBL was generally weak. A balloon that survived through the entirety of L2 was used to determine the airmass trajectory.

In this paper and Part II, we have attempted to bring together for the first time an integrated set of observations sufficient to provide both boundary conditions and verification data for MBL models and parameterizations that simulate the evolution of a moving marine air mass and its cloud cover. We hope that this Lagrangian observational strategy will help clarify our understanding of the melange of physical processes that interact to determine the structure and cloud cover of the marine boundary layer.

Acknowledgments. This work was supported by ONR Grant N00014-90-J-1136 and by NASA Global Change Research Fellowship 30047. The Lagrangian IOPs would not have happened without the untiring leadership of Dr. Bruce Albrecht of The Pennsylvania State University (ASTEX) and Barry Huebert of the University of Hawaii (MAGE). Balloon positions were provided by Dr. Steve Chiswell of North Carolina State University and Dr. Steve Businger of the University of Hawaii. Sounding data were provided by NCAR's Research Aviation Facility (Electra), Dr. Doug Johnson of the UKMRF (C130), and Dr. Dean Hegg of the University of Washington Cloud and Aerosol Research Group (C131a). Dr. Philip Austin of the University of British Columbia provided a C130 sounding and much invaluable advice. Dr. Steven Siems's help with the Electra data processing was invaluable, and Dr. Marcia Baker and her students helped process the C130 and C131a data. Steve Klein and Matt Wyant's careful reading and comments helped improve the manuscript.

REFERENCES

Albrecht, B. A., A. K. Betts, W. Schubert, and S. K. Cox, 1979: A model of the thermodynamic structure of the trade-wind boundary layer: Part I: Theoretical formulation and sensitivity tests. *J. Atmos. Sci.*, **36,** 73–89.

——, C. S. Bretherton, and D. Johnson, 1995: The Atlantic Stratocumulus Transition Experiment (ASTEX). *Bull. Amer. Meteor. Soc.*, in press.

Balke, D. R., O. W. Wingentner, M. K. Kubo, N. J. Blake, T. W. Smith Jr., and F. S. Rowland, 1995: Using NMHC and halocarbons as tracers during a Lagrangian experiment. *J. Geophys. Res.*, submitted.

Blomquist, B. W., A. R. Bandy, and D. C. Thornton, 1995: Sulfur gas measurements in the eastern north Atlantic Ocean during ASTEX/MAGE. *J. Geophys. Res.*, in press.

Bretherton, C. S., 1993: Understanding Albrecht's model of trade cumulus cloud fields. *J. Atmos. Sci.*, **50,** 2264–2283.

——, E. Klinker, J. Coakley, and A. K. Betts, 1995: Comparison of ceilometer, satellite and synoptic measurements of boundary layer cloudiness and the ECMWF diagnostic cloud parameterization scheme during ASTEX. *J. Atmos. Sci.*, **52,** 2736–2751.

Businger, S., S. Chiswell, W. C. Ulmer, and R. Johnson, 1995: The application of tetroons to meteorological problems. *J. Geophys. Res.*, in press.

Huebert, B. J., Pszenny, A. A. P., and B. W. Blomquist, 1995: An overview of the ASTEX/MAGE experiment. *J. Geophys. Res.*, in press.

Klein, S. A., and D. L. Hartmann, 1993: The seasonal cycle of low stratiform clouds. *J. Climate,* **6,** 1587–1606.

Pincus, R., M. Szczodrak, J. Gu, and P. Austin, 1995: Uncertainty in cloud optical depth estimates made from satellite radiance measurements. *J. Climate,* **8,** 1453–1462.

Zhuang, L., and B. J. Huebert, 1995: A Lagrangian analysis of the total ammonia budget during ASTEX/MAGE. *J. Geophys. Res.*, in press.